Ferrimagnetic Insulators for Spintronics: Beyond Garnets

Satoru Emori[1], Peng Li[2]

1. Department of Physics, Virginia Tech, Blacksburg, VA 24060 USA

2. Department of Electrical and Computer Engineering, Auburn University, AL 36849 USA

Ferrimagnetic insulators have gained much attention as platforms with efficient magnetization dynamics. To date, epitaxial iron garnet thin films are the most widely used materials in the emerging field of "insulator spintronics." However, further advances in this field require overcoming the disadvantages of garnets – e.g., their complex structure, high growth temperature, incompatibility with other crystalline materials, and relatively weak perpendicular magnetic anisotropy. In this Perspective Paper, we make the case that epitaxial thin films of *spinel ferrites* and *hexagonal ferrites* are viable materials for insulator spintronics, with complementary advantages over the oft-used garnets. Specifically, spinel ferrites have a simpler structure, can crystallize at lower temperatures, and are more amenable to coherent integration with various materials; hexagonal ferrites possess enormous perpendicular anisotropy of bulk origin, in contrast to garnets where the strength of anisotropy is restricted by interfacial strain. The expanded repertoire of materials for insulator spintronics will enable new physical insights and potential applications, beyond what is currently possible with garnets.

Corresponding authors: Satoru Emori (semori@vt.edu) and Peng Li (pzl0047@auburn.edu)

Section 1: Introduction

A flow of spin angular momentum injected into a magnetic thin film can exert torques on the magnetization [1,2]. Such spin-transfer torque effects were initially studied in heterostructures (e.g., spin valves and magnetic tunnel junctions), consisting of at least two layers of metallic ferromagnets [3]. An electric current flowing through the first conductive magnetic layer becomes spin-polarized and then imparts spin torques on the second conductive magnetic layer. In this scheme, the spin current that generates the spin torques is necessarily carried by the charge current.

In the last several years, alternative schemes to generate spin torques have been realized by taking advantage of spin-orbit coupling in nonmagnetic conductors. In one example, based on the spin-Hall effect in metals with strong spin-orbit coupling (e.g., Pt, β-W), conduction electrons in the metal undergo spin-dependent deflections such that spin-polarized electrons accumulate at the surfaces of the metal [4,5]. The spin-Hall effect generates a spin current (non-equilibrium spin accumulation) that is orthogonal to the input charge current, as illustrated in Figure 1. When this spin current transfers spin angular momentum to (or exchange couples with) the magnetization in an adjacent magnetic layer, torques are exerted on the magnetization. Similar spin torques may also emerge from spin accumulation due to spin-orbit coupling at the interface, i.e., Rashba-Edelstein effect [6–9].

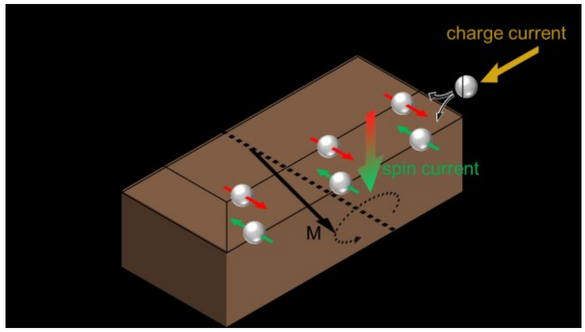

Figure 1. Spin current and torque generated from a charge current in the spin-orbit metal interfaced with a magnetic insulator. The spin dependent scattering of conduction electrons (e.g., spin-Hall effect) in the spin-orbit metal results in a spin current orthogonal to the charge current. The accumulation of spin-polarized electrons at the spin-orbit-metal/magnetic-insulator interface can exert torques on the magnetization, *M*.

Spin torques due to the spin-Hall (or Rashba-Edelstein) effect are often called "spin-orbit torques" (SOTs) [10]. Unlike conventional spin-transfer torques, SOTs do not require a charge current to enter the magnetic layer. SOTs instead rely on a spin current (or spin accumulation) orthogonal to the input charge current. Thus, SOTs can be exerted on magnetic moments in *insulators*.

SOTs allow for electrically controlling the magnetization in insulators, which are often thought to have lower magnetic damping than ferromagnetic metals. From the technological viewpoint, low damping allows for efficient excitation and propagation of magnetization dynamics with low energy input. For example, SOTs may be used to excite spin waves in magnetic insulators for magnonic computing and communications applications [11–13].

Magnetic insulators are also attractive for fundamental studies. With no parasitic effects from conduction electrons (which complicate analyses for structures with a conductive magnetic layer) [14–19], a magnetic insulator interfaced with a spin-orbit metal constitutes a simpler model system, particularly for determining the charge-spin interconversion processes in the spin-orbit metal. A magnetic insulator with low damping – or, more specifically, narrow ferromagnetic resonance (FMR) linewidths – boosts the signal-to-noise ratio for such experiments as spin-torque FMR and spin pumping [20], which are essential for quantifying the charge-spin interconversion efficiency. Alternatively, a magnetic insulator with perpendicular magnetic anisotropy (PMA) is a convenient platform for studying the dynamics of magnetization switching and domain wall motion driven by spin-orbit torques [6,21–23]. In other words, appropriate magnetic insulators can serve as sources of spin currents (transferred from the magnet to the spin-orbit metal, i.e., in spin pumping measurements) or detectors of spin currents (transferred from the spin-orbit metal to the magnet, i.e., in spin-torque measurements).

Magnetic insulators are often presumed to exhibit low damping because spin scattering processes from conduction electrons are absent [24,25]. There exist many families of magnetic insulators – particularly Fe-based ferrimagnetic oxides or "ferrites" – with a variety of crystal structures [26,27]. One might therefore expect a large selection of thin-film insulating materials used for spintronic applications. In reality, one family of magnetic insulators – garnet ferrites – has dominated the growing research field of insulator spintronics. The reason for this is in part historical: a garnet ferrite, i.e., yttrium iron garnet (YIG), has been widely known as the material with the lowest damping (since the 1950s [28]), with a Gilbert damping parameter $\sim 10^{-5}$ for bulk YIG crystals. There have been accordingly numerous studies in the past decade demonstrating ultralow damping parameters on the order of $\sim 10^{-4}$ for epitaxial YIG thin films [20,29–38], grown on single-crystal gadolinium gallium garnet (GGG) substrates that are very well lattice-matched to YIG. Many of these ultralow-damping YIG thin films have been used in spin pumping and spin torque experiments [20,39–42]. Further, garnets ferrites with tunable PMA (e.g., thulium iron garnet, terbium iron garnet, etc.) have also gained considerable attention as media for insulator spintronics, especially with regards to chiral magnetism. (We point out, however, that low damping is not necessarily a prerequisite for low-power SOT switching of PMA media [43].)

While widely used in insulator spintronics, there are some drawbacks to the garnet ferrites.

1. They have a complex structure with three sublattices and an enormous unit cell consisting of 160 atoms.
2. They require a high thermal budget to crystallize, e.g., deposition and/or post-anneal at > 700 ºC.
3. They cannot be readily interfaced with other classes of crystalline materials.
4. The magnitude of PMA is modest (e.g., a few kOe) in garnets, and it is strongly dependent on the strain between the magnetic film and the substrate [21].

The above considerations bring up a natural question: are there alternative types of ferrimagnetic insulators that can be used in place of the oft-used garnets?

In this Perspective Paper, we present two alternative families of ferrimagnetic insulators as viable – or possibly superior – platforms for insulator spintronics. In Section 2, we outline recent experimental studies on high-quality, coherently strained epitaxial thin films of *spinel ferrites*. These new thin-film ferrites mitigate the first three drawbacks of garnet ferrites listed above. They can therefore serve as useful model-system materials – simpler and more convenient than garnets – to study spin dynamics and transport. For instance, a recently reported spinel ferrite system [44] exhibits sufficiently low damping that enables spin pumping and SOT experiments giving insights into charge-spin interconversion in epitaxial Pt [45,46]. In Section 3, we summarize recent experiments leveraging epitaxial thin films of *hexagonal ferrites* with PMA that is much stronger than that of typical garnet ferrites. These out-of-plane magnetized hexaferrites have a strong anisotropy field of ~ 17 kOe and a low intrinsic damping constant <0.001 [47]. Finally, in Section 4, we briefly offer our perspectives on challenges associated with using these magnetic insulator thin films for practical device applications.

Our Perspective Paper primarily focuses on the thin-film spinel ferrites and hexagonal ferrites in the context of spintronics. For more general and detailed accounts of the different families of ferrites, we refer the reader to the review articles by Harris [26] and Pardavi-Horvath [27]. Overall, we hope that this Perspective Paper will inspire the growing field of insulator spintronics to expand its materials repertoire beyond garnet ferrite films. We believe that this "beyond-garnet" perspective will further advance fundamental insights and potential applications of thin-film magnetic insulators.

Section 2: Coherently Strained Epitaxial Spinel Ferrites

2.1: Spinel Ferrites for Spintronics: General Considerations

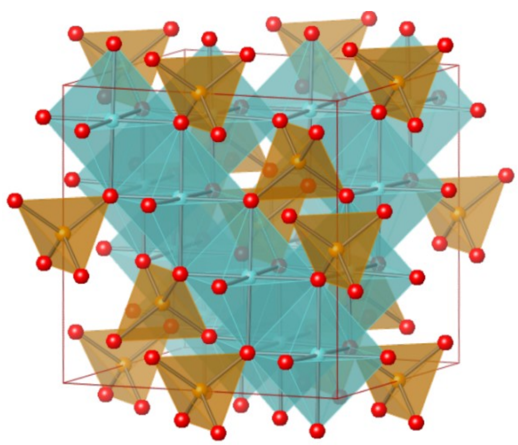

Figure 2. Schematic of the spinel structure. The tetrahedrally coordinated cations are represented by the brown spheres, whereas the octahedrally coordinated cations are represented by the blue spheres. The oxygen anions are represented by the red balls.

The spinel is a cubic crystal (schematic in Fig. 2) with the general single formula unit usually written as AB_2O_4 (e.g., $MgAl_2O_4$), where A represents divalent cations (e.g., Mg^{2+}) at lattice sites tetrahedrally coordinated by oxygen anions and B (e.g., Al^{3+}) represents trivalent cations at lattice sites octahedrally coordinated by oxygen anions. Many spinel ferrites (e.g., Fe_3O_4, $NiFe_2O_4$) are so-called "inverted" spinels where the divalent cations (e.g., Fe^{2+}, Ni^{2+}) preferentially occupy the octahedral B sites, such that half of the trivalent cations (e.g., Fe^{3+}) are at the tetrahedral A sites. We refer the reader to Harris [26] and Pardavi-Horvath [27] for more detailed discussions of the chemistry, structure, and magnetic order of spinel ferrites.

Spinel ferrites comprise many naturally occurring magnetic minerals, with "lodestone" (magnetite, Fe_3O_4), perhaps being the most well-known from the ancient civilizations of China and Greece. While Fe_3O_4 is a room-temperature ferrimagnetic semiconductor (exhibiting interesting phenomena such as the Verwey phase transition and half-metallicity), there are plenty of ferrimagnetic spinel ferrites that are electrically insulating (e.g., $Li_{0.5}Fe_{2.5}O_4$, $MgFe_2O_4$, $NiFe_2O_4$, $CoFe_2O_4$, etc.). Many such insulating spinel ferrites [26,27] have been widely used in microwave device applications for decades. Despite their long history, spinel ferrites have not made inroads into the emerging field of insulator spintronics. This is perhaps surprising considering the relative simplicity and other advantages of the spinel compared to the notoriously complicated garnet. One might then imagine that spinel ferrites should constitute a more convenient model system for insulating spintronics.

A major problem with spinel ferrite films – or, for that matter, essentially many other ferrimagnetic oxide films (other than YIG) – is that magnetization dynamics is typically too lossy, i.e., the FMR linewidth or effective damping is too large. The high loss in these ferrite films largely comes from structural defects, such as antiphase boundaries and dislocations [48–54], which are known to be sources of extrinsic spin dissipation, e.g., two-magnon scattering [49,50,52,55,56]. Further, these defects lead to nonuniform magnetic states [44,48,51,53] that may contribute to inhomogeneous resonance linewidth broadening [24,56]. Overall, conventional spinel ferrite films typically exhibit broad linewidths greater than 100 Oe at X-band (~10 GHz), or effective Gilbert damping parameters in excess of 0.01 [49–53]. We remark that these insulating ferrite films have higher effective damping than many commonly used ferromagnetic metals. *Being insulating is evidently not sufficient to achieve low loss.*

Minimizing structural defects in spinel ferrite thin films appears to be key to lower loss. To prevent the formation of antiphase boundaries, the film needs to be grown on a matching substrate, specifically a high-quality single-crystal spinel – as opposed to often-used rock-salt MgO or perovskite $SrTiO_3$ substrates [48–51]. This requirement means that spinel-structure $MgAl_2O_4$ is essentially the only viable substrate, since $MgAl_2O_4$ is the only spinel that is commercially available as single-crystal substrates. Further, the spinel ferrite film must be *pseudomorphic* [44,53,54,57]: the lattice parameters of the film and substrate must be close enough that the film can remain coherently strained to the substrate, without structurally relaxing (e.g., forming dislocations), as illustrated in the exaggerated cartoon in Fig. 3(a). Unfortunately, the lattice parameters of conventional spinel ferrites (typical lattice parameters $a \approx 8.35$-8.5 Å) [26,27] are too large compared to that of $MgAl_2O_4$ ($a = 8.08$ Å). The resulting lattice mismatch of >3%

makes it very challenging to grow high-quality, pseudomorphic thin films of spinel ferrites with sufficiently low loss.

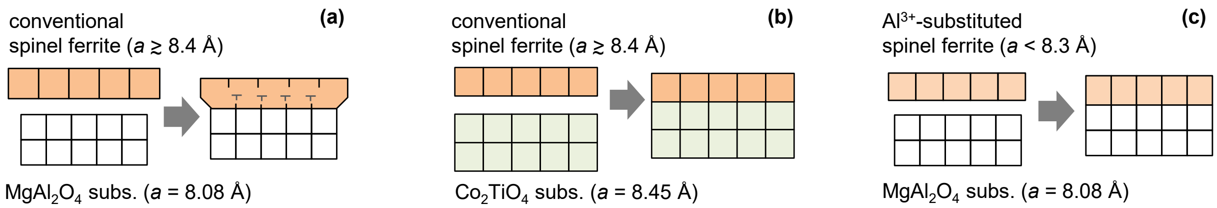

Figure 3. Cartoon schematics of lattice matching between spinel ferrite films and spinel substrates. (a) The conventional spinel ferrite has a significant lattice mismatch with the commercially available $MgAl_2O_4$ substrate, thereby resulting in a relaxed film with a high density of defects (e.g., dislocations). (b) A coherent epitaxial film of conventional spinel ferrite can be grown on an alternative lattice-matched spinel substrate, but such a substrate is not widely available. (c) A novel spinel ferrite with a reduced lattice parameter, enabled by partial substitution of Fe^{3+} with Al^{3+}, can be grown on the $MgAl_2O_4$ substrate to produce a coherent epitaxial film.

One obvious solution to the above issues is to use spinel substrates that are well lattice-matched to conventional spinel ferrites (Fig. 3(b)). A few recent studies have demonstrated pseudomorphic spinel ferrite films grown on such spinel substrates as $MgGa_2O_4$, $CoGa_2O_4$, and Co_2TiO_4, with lattice parameters of 8.28 Å, 8.33 Å, and 8.45 Å, respectively [53,54,58]. However, this approach requires substrate-grade crystals of these spinels, which are currently available from only a limited number of laboratories. Thus, for the time being, high-quality epitaxial growth of conventional spinel ferrites is hindered by the restricted availability of appropriate single-crystal spinel substrates.

Here, we focus on an alternative solution where the lattice parameter of the spinel ferrite is reduced to better match the commercially available $MgAl_2O_4$ substrate, as illustrated in Fig. 3(c). The smaller lattice parameter is achieved by replacing some of the Fe^{3+} cations in the ferrite with Al^{3+}, which has a smaller ionic radius than Fe^{3+}. Recent studies have demonstrated high-quality growth of such Al^{3+}-substituted spinel ferrite films [44,57,58], which provide an intriguing alternative to complement iron garnets in insulator spintronics. Advantages of these high-quality spinel ferrite thin films include the following:

- The spinel unit cell (56 atoms) is smaller than the garnet unit cell (160 atoms). Spinel ferrites contain only two magnetic sublattices, whereas iron garnets host up to three magnetic sublattices. The ferrimagnetism of spinel ferrites remains comparatively simple even with chemical substitution, in contrast with iron garnets that exhibit increasingly complex noncollinear ferrimagnetism in some cases [59,60]. Spinel ferrites may therefore serve as simpler model systems compared to iron garnets.

- Spinel ferrites can be crystallized at lower temperatures compared to iron garnets. A temperature range of ~300-500ºC is typical for spinels, in contrast to epitaxial YIG, which requires deposition and/or annealing at 700-850ºC for crystallization. The lower growth temperature for epitaxial spinels may be attractive for reducing thermal budgets or making the ferrite growth process compatible with processing steps in practical device fabrication. The lower temperature may also help reduce atomic intermixing across interfaces, thus allowing for sharper, more coherent interfaces. For instance, magnetic dead layers at spinel substrate/film interfaces are only ~1 nm thick [61,62], in contrast to several-nm-thick dead layers that have been reported for garnet substrate/film interfaces [63,64].
- Spinel ferrites, particularly those grown coherently on $MgAl_2O_4$, are well lattice-matched with some of the widely-used or interesting materials in spintronics. Examples of materials that may be grown epitaxially on top of spinels include Pt [46,65], (Co)Fe [66,67], and NiO [68,69]. Such all-epitaxial ferrite-based bilayers can serve as ideal model systems to explore spintronic phenomena in the structurally clean limit. Highly crystalline composites of spinels with perovskites are also possible [70,71]; this points to the possibility of all-oxide epitaxial multilayers, consisting of a spinel ferrite interfaced coherently with a perovskite system exhibiting intriguing correlated phenomena. By contrast, metal and (non-garnet) oxide films grown on top of iron garnets are typically polycrystalline or amorphous.
- Coherently strained spinel ferrites (e.g., tetragonally distorted) can exhibit large strain-induced magnetic anisotropy [57]. When the large strain-induced anisotropy is easy-plane, the resonance frequency (for in-plane FMR) is increased at a given external field, and the group velocity for magnetostatic spin waves can be increased [36,72]. For example, coherently strained low-damping spinel ferrite thin films (discussed further below) require an in-plane magnetic field of only < 1 kOe for 10-GHz resonance response, compared to ≈2.5 kOe for YIG [29–31,34,73]. This lower field requirement for high-frequency resonance may be advantageous for compact, high-bandwidth spintronic and magnonic devices. Further, by either reversing the sign of the strain or the magnetoelastic coupling, it is possible to achieve perpendicular magnetic anisotropy in spinel ferrites [58].

In the following, we briefly discuss a few examples of recent studies on coherently strained epitaxial spinel ferrites grown on $MgAl_2O_4$. The unique features and advantages of these epitaxial ferrite films are emphasized from the perspective of thin-film spintronics.

2.2: Low-Damping Spinel MgAl-Ferrite

Among Al^{3+}-substituted spinel ferrite films, MgAl-ferrite ($MgAl_{0.5}Fe_{1.5}O_4$, MAFO) possesses highly desirable properties as low-damping insulating media [44,74]. With the nominal Al^{3+}:Fe^{3+} ratio of 1:3, the concentration of magnetic Fe^{3+} is still high enough that the Curie temperature (≈400 K) is well above room temperature, while the lattice mismatch between MAFO and $MgAl_2O_4$ is reduced to ≈2% (with the lattice parameter of MAFO, $a \approx 8.24$ Å). Pseudomorphic (coherently strained) growth of MAFO on $MgAl_2O_4$ is maintained up to a film thickness of ≈20 nm.

In addition to the high crystalline quality of the film, another important consideration for achieving low damping in magnetic insulators is the reduction of intrinsic spin-orbit coupling [75]. Simply put, the idea is to minimize the dissipative pathway from magnetization dynamics to lattice excitations. In this regard, MAFO is an excellent choice, as it consists of cations with nominally zero orbital angular momentum ($L = 0$) and, hence, minimal spin-orbit coupling. The weak orbital contribution to magnetism in MAFO is in part corroborated by its effective g-factor (≈2.05) of close to the spin-only value of 2.0.

One could actually think of MAFO as a spinel analog of YIG. First, similar to high-quality epitaxial YIG grown on the well-lattice matched GGG substrate, MAFO is reasonably lattice-matched to the isostructural $MgAl_2O_4$ – such that high-quality pseudomorphic epitaxial growth is attained. However, the ≈2% lattice mismatch with $MgAl_2O_4$ does lead to a rather large tetragonal distortion $c/a \approx 1.06$ in MAFO, whereas YIG on GGG is essentially cubic. The impact of tetragonal distortion on damping in coherently strained MAFO is yet unclear. Second, just as the cations in YIG (Y^{3+}, Fe^{3+}) are stable and have $L = 0$, the Mg^{2+}, Al^{3+}, and Fe^{3+} cations in MAFO are also stable with $L = 0$. In both YIG and MAFO, what appears to be crucial to the low intrinsic damping (low spin-orbit coupling) is that Fe^{3+} with half-filled orbital shells and the high-spin configuration ($L = 0$) serves as the sole source of magnetism.

Recent experimental studies report coherently strained MAFO films with low Gilbert damping parameters of $\alpha \sim 0.001$-0.002 [44–46,62,74], at least an order of magnitude lower than the effective damping parameter >0.01 for typical spinel ferrite films. The damping parameter of coherently strained MAFO is also comparable to those of the lowest-damping spinel ferrite bulk crystals [76]. Figure 4 shows how the frequency dependence of FMR linewidth compares among thin films of coherently strained MAFO, coherently strained YIG, polycrystalline metallic $Ni_{80}Fe_{20}$, and partially relaxed spinel MnZn-ferrite (similar to those reported in Ref. [77]). It should be noted that while MnZn-ferrite nominally has the $L = 0$ cation chemistry, the large linewidths and the nonlinear frequency dependence point to strong two-magnon scattering due to substantial structural disorder (structural relaxation) from the large lattice mismatch with the substrate (cf. Fig. 3(a)) [48–54]. Although $\alpha \sim 0.001$ for MAFO is still about over an order of magnitude higher than the lowest reported for YIG films [20,29–38], MAFO thin films have narrow FMR linewidths <10 Oe at ~10 GHz, comparable to low-damping YIG. The narrow linewidths are enabled by minimal inhomogeneous broadening, resulting in a small zero-frequency linewidth. We also remark that $\alpha \sim 0.001$ is often low enough for many studies on spintronic phenomena (e.g., SOTs) in magnet/spin-orbit-metal bilayers, as a magnetic thin film interfaced with a spin-orbit metal exhibits a Gilbert damping enhancement $\Delta\alpha_{sp}$ that is a few times larger than ~0.001 due to spin pumping [20] (and possibly other interfacial scattering mechanisms [62,78]). In that regard, it may not be so consequential to have $\alpha << 0.001$ for a bare ferrite thin film for SOT-driven applications.

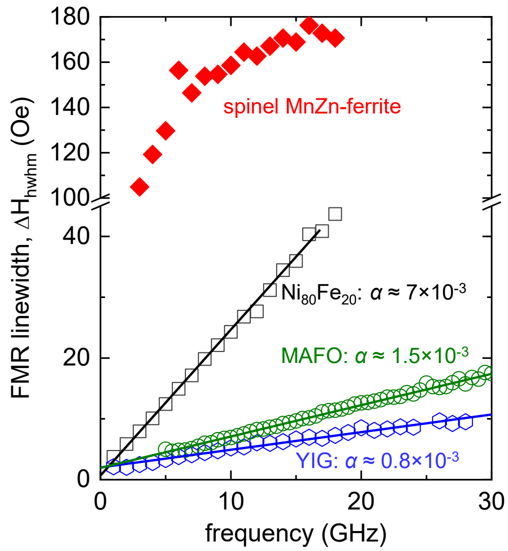

Figure 4. Frequency dependence of FMR linewidth for thin films of MAFO, YIG, metallic $Ni_{80}Fe_{20}$, and spinel MnZn-ferrite. Note the much larger linewidths for MnZn-ferrite (a conventional spinel ferrite film grown on $MgAl_2O_4$, cf. Fig. 3(a)), likely due to strong two-magnon scattering arising from defects.

Notably, the effective damping parameters (or FMR linewidths) of MAFO films – and other epitaxial spinel ferrite thin films reported recently – diverge at large film thicknesses, accompanied by the onset of structural relaxation [44,57,61,79]. For instance, it can be seen from the X-ray diffraction reciprocal space maps in Fig. 5(a) that 18-nm-thick MAFO is coherently strained to the $MgAl_2O_4$ substrate (i.e., the in-plane lattice parameters of the film and substrate match), whereas 40-nm-thick MAFO is partially relaxed (i.e., the in-plane lattice parameters of the film and substrate do not match). The FMR linewidths of partially relaxed MAFO are an order of magnitude larger compared to those of thinner, coherently strained films [44,61], as shown in Fig. 5(b). The FMR linewidths of thicker, structurally relaxed MAFO films are also strongly anisotropic (Fig. 5(c)), pointing to a strong contribution from two-magnonscattering. These observations highlight the crucial role played by the structural quality of the ferrite film: effective damping (FMR linewidths) in ferrite films is highly sensitive to structural defects. A potentially interesting future research direction is to determine whether thin films of MAFO (or perhaps other $L = 0$ ferrites, e.g., $MgFe_2O_4$, $Li_{0.5}Fe_{2.5}O_4$) with much smaller tetragonal distortion (i.e., by growing on better lattice-matched spinel substrates) may exhibit even lower damping.

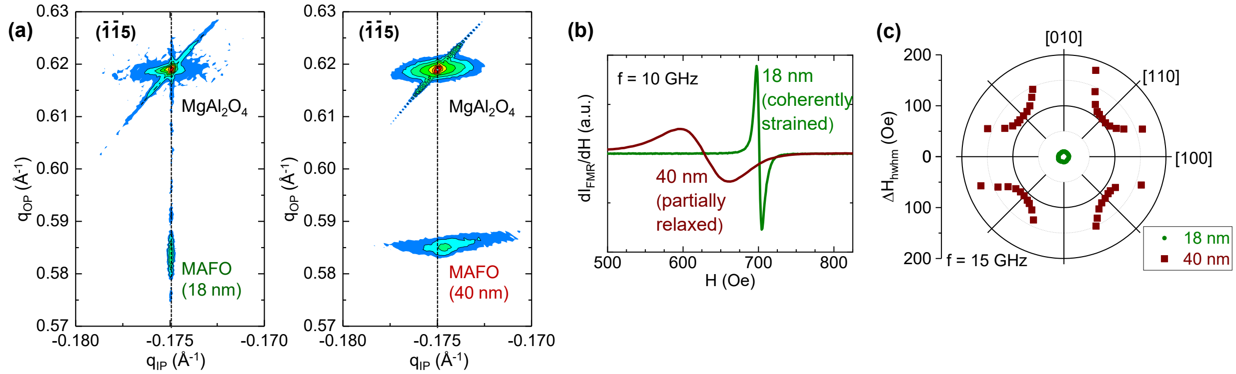

Figure 5. (a) Reciprocal space maps of 18- and 40-nm-thick spinel MgAl-ferrite (MAFO) films on $MgAl_2O_4$ (001) substrates. The in-plane lattice parameter of the 18-nm-thick MAFO film coincides with that of the $MgAl_2O_4$ substrate, indicating coherently strained film growth. By contrast, the offset in in-plane lattice parameter and the smeared peak for the 40-nm-thick MAFO film indicates partially relaxed film growth. (Reprinted with permission from Ref. [44]. Copyright (2018) American Chemical Society). (b) FMR spectra (at 10 GHz), and (c) FMR linewidth ΔH_{hwhm} vs. in-plane field angle of the 18-nm-thick coherently strained MAFO film and the 40-nm-thick partially relaxed MAFO film. The wider FMR linewidth and its pronounced anisotropy for the 40-nm-thick film suggest significant two-magnon scattering due to defects within the film.

In addition to the structural properties of ferrite films, the ferrite cation chemistry governs the magnitude of intrinsic damping. For instance, NiZnAl-ferrite ($Ni_{0.65}Zn_{0.35}Al_{0.8}Fe_{1.2}O_4$, NZAFO), where the more complex cation chemistry may lead to a deviation from $L = 0$, exhibits a higher damping parameter ($\alpha \sim 0.003$) [57,58] than MAFO. In all ferrite films, another likely important – and subtle – factor is the deviation from the nominal stoichiometry, such as the presence of Fe^{2+} (e.g., due to incomplete oxidation of Fe and imperfect stoichiometry transfer from the target to the film). While prior studies conclude that the magnetism of MAFO predominantly arises from Fe^{3+} (i.e., based on X-ray absorption spectroscopy) [44,74], it is conceivable that a small concentration of Fe^{2+} (i.e., below the sensitivity of XAS) still plays a key role. There is some evidence that subtle off-stoichiometry has substantial impact on damping, e.g., in MAFO. Ref. [44] notes that consistently lower damping was achieved in pulse-laser-deposited MAFO by placing the substrates ≈10 mm away from the center of the ablated plume, which might be due in part to a gradient in the composition of the plume. Another study where 15-nm-thick MAFO is interfaced with a thin layer of an insulating paramagnetic spinel ($CoCr_2O_4$) shows a large (≈3-fold) increase in damping, even though the $CoCr_2O_4$/MAFO is structurally pristine [62]. In Ref. [62], the enhanced damping is attributed to the ultrathin (at most ≈1 nm thick) chemically disordered layer at the

$CoCr_2O_4$/MAFO interface, implying a significant impact of off-stoichiometry on damping. It is our hope that future studies will further reveal the fundamental atomic-scale interplay between the cation chemistry and magnetization dynamics in ferrite thin films.

2.3: Spinel Ferrites as Platforms for Spin Transport Studies

A low-damping ferrite can be interfaced with a spin-orbit metal to make a convenient model system, particularly for studying charge-spin interconversion processes in the metal through FMR-based methods. Low damping (or narrow FMR linewidth) is especially important for a high FMR signal and hence measurement sensitivity. For instance, we can reliably measure how a DC bias current through the spin-orbit metal modifies the spin-torque FMR spectrum of the low-damping magnetic layer [80,81]. The efficiency of the damping-like SOT (field-like SOT) can be quantified straightforwardly from the linear change of FMR linewidth (resonance field) with DC current. Moreover, the insulating nature of the ferrite ensures that the charge current passes only through the metal, and that proximity induced magnetism in the adjacent metal layer is weak or practically absent [82]. We can therefore avoid any complications that generally arise from oft-used ferromagnetic metals [18,19] – and instead probe SOTs that arise solely from the spin-orbit metal. In essence, a low-damping ferrite can be used as a sensor for spin angular momentum injected from (or into) the adjacent metal via SOTs (or spin pumping).

Among low-damping ferrites, a unique advantage of coherently strained epitaxial MAFO is that its in-plane lattice parameter (a = 8.08 Å, identical to that of the spinel $MgAl_2O_4$ substrate) matches well with the crystals of a variety of materials that are of interest for spintronics. This allows us to study charge-spin interconversion processes in highly crystalline materials, which may be more amenable to direct comparison with theoretical predictions. One example of such materials well lattice-matched with MAFO is FCC Pt (Fig. 6), particularly with an out-of-plane crystallographic orientation of (111), the closest packed plane of the FCC crystal structure. The fortuitous matching between the Pt (111) hexagonal lattice and the square spinel (001) lattice (i.e., Pt(111) [110] || MAFO(001) [110], as shown in Fig. 6(d)) enables epitaxial growth of (111)-oriented Pt with exceptionally high crystalline quality on (001)-oriented MAFO [65] – even when the Pt overlayer is sputter-deposited at room temperature [46]. The epitaxial Pt on MAFO is in stark contrast to the polycrystalline or amorphous structure of Pt that results from growth on top of YIG. The all-epitaxial Pt/MAFO interface is also atomically sharp without substantial intermixing [46]. The Pt/MAFO bilayer is, therefore, a "clean" model system, where charge-spin interconversion is restricted to the highly crystalline Pt layer.

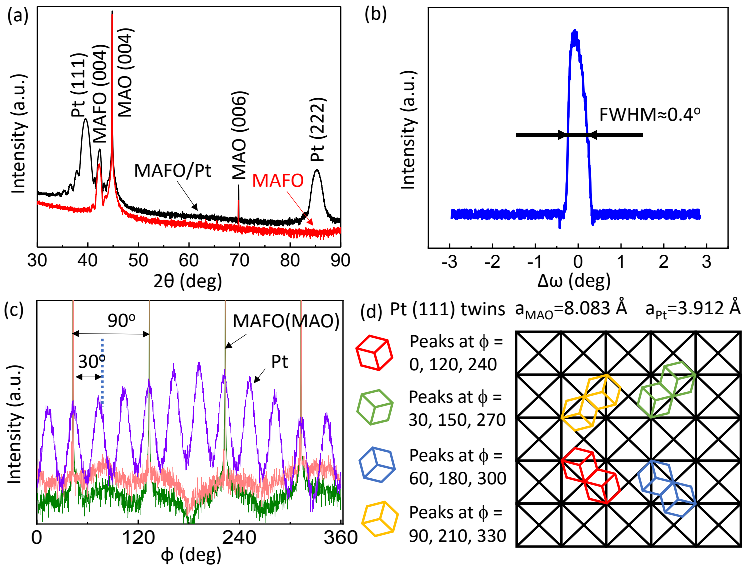

Figure 6. Structure characterization of Pt (5 nm)/MAFO (13 nm) and MAFO (13 nm). (a) XRD 2θ/ω scans. The Laue oscillations around the Pt(111) film peak indicate a smooth Pt/MAFO interface. Note that $MgAl_2O_4$ is abbreviated as MAO here. (b) Rocking curve scan about the Pt (111) peak for the Pt/MAFO bilayer shown in (a). The narrow width indicates minimal mosaicity in the Pt film grown on MAFO. (c) XRD φ scans on the (113) plane of multilayer in the MAFO (13 nm)/Pt (5 nm) sample. Pink: MAFO film. Green: $MgAl_2O_4$ (MAO) film. The MAFO film and $MgAl_2O_4$ (MAO) substrate exhibit four maxima, expected from its in-plane four-fold symmetry (cubic structure). The Pt(113) peak exhibits twelve maxima due to the twinning of the Pt domains, as illustrated in (d). (d) Lattice matching relationship between the Pt and MAFO (MAO) unit cells. There are four possible orientations for the Pt domains, and each domain has three-fold in-plane symmetry, thereby producing a total of twelve peaks in the XRD φ in (c). Adapted from Ref. [46]. Originally published under nonexclusive-distrib 1.0 license.

In addition to Pt, there are other materials well lattice-matched with MAFO that may constitute interesting crystalline model systems for spintronics. It has been demonstrated that exceptionally high-quality Fe and CoFe can be grown on spinel $MgAl_2O_4$ [66,67], which implies that coherent (Co)Fe/MAFO bilayers can be readily grown. Such all-epitaxial (Co)Fe/MAFO may be useful for studying magnon-magnon coupling [83] in the presence of substantial magnetocrystalline anisotropy. Though not demonstrated yet, coherently strained epitaxial growth of antiferromagnetic NiO (a = 4.17 Å) on top of the spinel (a/2 = 4.04 Å) may be feasible and open possibilities for better understanding the basic mechanism of efficient spin transport in antiferromagnetic insulators [84–86]. Moreover, considering reports of two-dimensional electron gases with strong Rashba effects at spinel/perovskite interfaces [70,71], all-epitaxial spinel-ferrite/perovskite heterostructures may unlock novel physics of spin transport. Overall, high-quality epitaxial spinel ferrites hold untapped potential as model-system platforms to examine a variety of spin-driven phenomena.

2.4 Spinel Ferrite as a Two-Sublattice Model System

Practically all magnetic insulators that exhibit a substantial net magnetization at room temperature are *ferrimagnetic* [26,27], consisting of two (or more) magnetic sublattices that are antiferromagnetically coupled. This means that the net magnetization (or net angular momentum) of ferrimagnetic insulators can be made close to zero when the magnetic moments (or angular momenta) of the magnetic sublattices compensate each other. Such ferrimagnetic compensation can be achieved by tuning the magnetic cation composition of the sublattices. While recent experiments have reported enhanced magnetization dynamics (e.g., higher domain wall and skyrmion mobilities, higher SOT efficiencies) in *metallic* compensated ferrimagnets [87], insulating ferrites may serve as intriguing alternative platforms for fundamental studies of how a spin current (e.g., carried by magnons) interacts with compensated magnetic order. Nearly compensated ferrites – whose magnetization can be controlled and probed by an external magnetic field – may complement experimental studies of antiferromagnetic insulators, where the alignment and characterization of magnetic order can be rather difficult.

A preliminary study by one of the present authors points to epitaxial thin films of NiAl-ferrite (NiAFO, $NiAl_xFe_{2-x}O_4$, bulk crystals originally studied in the 1950s [88]) as ideal insulating materials exhibiting compensated ferrimagnetism. As in all other spinel ferrites, the magnetic sublattices of NiAFO consist of tetrahedrally-coordinated and octahedrally-coordinated magnetic cations. Since there are twice as many octahedrally-coordinated sites, the net magnetization in most spinel ferrites is dominated by the octahedral magnetic sublattice. This is indeed the case for NiAFO with low Al^{3+} content. However, beyond a threshold content of Al^{3+} (which prefers to occupy the octahedral sites), the tetrahedral magnetic sublattice dominates over the octahedral sublattice. Preliminary X-ray magnetic circular dichroism results indeed confirm the reversal of the dominant magnetic sublattice in NiAFO at an Al^{3+}:Fe^{3+} ratio of above 0.8. Remarkably, the Curie temperature remains well above room temperature even at a high Al^{3+}:Fe^{3+} ratio of 1, thus making this material system suitable for accessible room-temperature spin transport experiments. We further note that spinel ferrites (56 atoms/unit cell, two magnetic sublattices) are simpler ferrimagnets than iron garnets (160 atoms/unit cell, up to three magnetic sublattices [59,60]) and therefore facilitate the analysis of experimental results. NiAFO is a relatively simple two-sublattice system that may provide a new research pathway in insulator spintronics. For instance, while ferrites are often treated as ferromagnets (i.e., by considering the dynamics of the net magnetization), the two-sublattice ferrite may facilitate new experiments, combined with effective macrospin modeling, to uncover dynamical effects (possibly in the ultrafast THz regime) governed by antiferromagnetic exchange coupling between the sublattices [89,90].

Section 3: Barium Hexagonal Ferrite for Spin-Orbit Torque Devices

3.1 General Properties of Hexagonal Ferrites

Hexagonal ferrites consist of a subfamily with different types (M, Z, Y, W, X, U types) [91]. They have a general formula of $A_xMe_yFe_zO_i$, where A can be Ba or Sr, Me can be Co^{2+}, Ni^{2+}, Zn^{2+}. They all have strong magnetocrystalline anisotropy, such that some have an easy axis along the *c*-axis while others have easy-plane or cone anisotropy.

Among the hexagonal ferrites, M-type barium hexagonal ferrite $BaFe_{12}O_{19}$ (noted as BaM) has a large crystalline anisotropy field ~17 kOe along the *c* axis. Each unit cell of BaM has a net magnetic moment of $40\mu_B$. The *a* and *c* axes of a BaM unit cell are 5.89 Å and 23.2 Å, respectively. Based on those values, the saturation magnetization ($4\pi M_s$) of BaM is estimated to be ~6680 G, which is consistent with the reported value from the experiments [92]. For more information on the BaM structure, we refer the reader to Refs. [47,92,93].

BaM has many advantages for spintronic experiments. For the CoFeB/MgO structure that is often used in a magnetic tunnel junction, the CoFeB layer thickness is usually limited to < 1 nm to maintain a strong interfacial anisotropy [94]. This thickness limit for BaM does not apply because the bulk anisotropy facilitates a flexible thickness for device applications. Moreover, the intrinsic Gilbert damping constant in BaM materials is 7×10^{-4} [47], which is an order of magnitude smaller than that of ultrathin CoFeB. Thus, BaM may be attractive for spin-torque oscillator applications, where the current threshold for self-oscillations decreases with the damping, as well as for logic device applications. The Curie temperature of bulk BaM is 725 K, much higher than room temperature [47]. In fact, BaM has found their use as permanent magnets, microwave devices, and recording media. Recently, there has been an increasing interest in using M-type barium hexagonal ferrite for spintronic devices [96,112]. In the following, we introduce representative spin transport experiments that take advantage of some of the exotic properties of BaM.

3.2 Spin-Orbit Torque Switching in Heavy Metal/Hexagonal Ferrite Bilayers

The spin Hall effect has enabled current-induced switching in nonmagnetic heavy metal (HM)/ferromagnetic metal (FM) heterostructures. In this case, the current induces a SOT that exerts on FM and causes the magnetization switching [95,96]. It was found that SOT is strongly dependent on the matching of the band structures of the HM and FM metals at the interface [97]. Will this mechanism hold for an HM/magnet structure in which the magnet is insulating? This question has spurred a strong interest in studying SOT switching in an HM/magnetic insulator (MI) structure. Such experiments were not realized for a long time, challenged by both identifying a proper MI with PMA and a convenient way to read the magnetization states.

There are several candidates as PMA MIs. For example, garnets such as $Tm_3Fe_5O_{12}$ and $Eu_3Fe_5O_{12}$ gain PMA from the interfacial lattice strain between the film and the substrate [21,95]. The drawback of using such a PMA garnet is that the thickness has to be controlled precisely. As mentioned above, the hexagonal ferrites have more flexibility in the thickness of device applications. Moreover, BaM has a much stronger anisotropy field (~17 kOe) than that (2.7 kOe) of PMA garnets. Thus BaM can survive the superparamagnetic limit further when they are patterned into small magnets for magnetic memory purposes. These advantages have made the hexagonal ferrites a unique material for SOT switching devices.

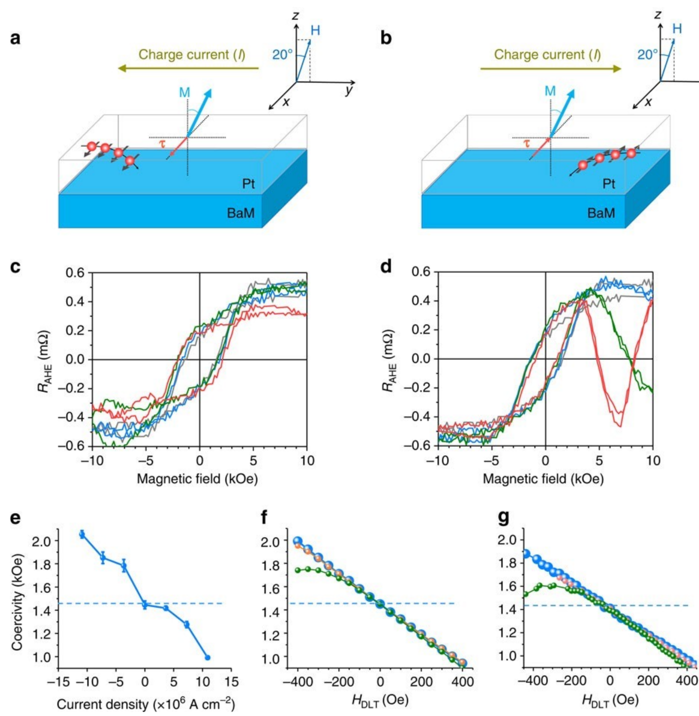

Figure 7. Switching responses in Pt/BaM for out-of-plane magnetic fields. (a) and (b) show the configuration of charge current (I), magnetization (M), external field (H) and spin polarization (τ). The red balls represent spin-polarized electrons from spin Hall effect. (c) and (d) show the dependence of anomalous Hall resistance R_{AHE} of the Hall bar on the magnetic field at different charge currents. Grey: I = 0; Blue: I = −2 mA; Olive: I = −4 mA; and Red: I = −6 mA. In (d) Grey: I = 0; Blue: I = 2 mA; Olive: I = 4 mA; and Red: I = 6 mA. (e) The measured coercivity of the BaM film as a function of the charge current density. (f) and (g) Coercivity versus damping-like torque field (H_{DLT}) estimated for three different field-like torque fields (H_{FLT}) through macrospin and micromagnetic simulations, respectively. Large blue spheres: H_{FLT}=0; small red spheres: H_{FLT}=H_{DLT}/2; and small olive spheres: H_{FLT}=H_{DLT}. The dash line in (e–g) is the H_c at I = 0. Adapted from Ref. [98].

In a SOT switching experiment [98], the authors chose Pt as the nonmagnetic HM, which was sputtered onto a 3 nm BaM thin film made in a pulsed laser deposition system. A DC current in the Pt layer induced a SOT, which switched the BaM magnetization. It was found that the switching response in the

BaM film strongly depends on the charge current applied to the Pt film [98]. As shown in Figure 7, when a constant magnetic field is applied in the film plane, the charge current in the Pt film exerted damping-like

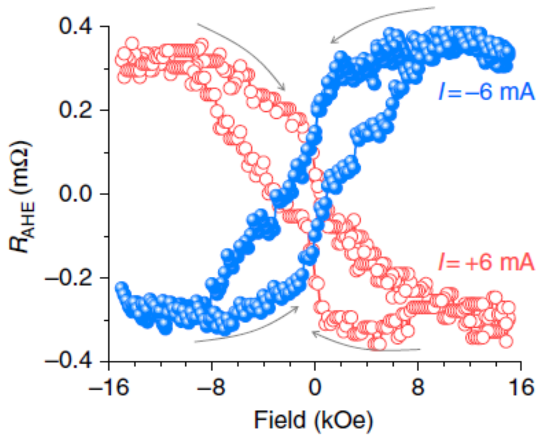

Figure 8. Anomalous Hall resistance R_{AHE} measured as a function of a magnetic field along the y axis for $I = +6$ mA and $I = -6$ mA, respectively. The grey arrows indicate opposite evolution of the switching loops under charge currents of different polarities. This result provides a strong evidence for the presence of the SOT at the interface.Adapted from Ref. [98].

and field-like torques on the magnetization ($\mathbf{M}_z$) in the BaM film. The damping-like torque either counters/aligns with the torque produced by the external magnetic field and thereby hinders/assists the switching of the magnetization **M** in the BaM film. This effect is clearly evident by the broadening/narrowing of the anomalous Hall effect hysteresis loop with increasing current. When the coercivity is measured by sweeping an out-of-plane field, its value can be reduced or increased by as much as about 500 Oe if an appropriate charge current is applied.

The current also dictates the up and down states of the remanent magnetization when the in-plane field is reduced to zero. Figure 8 shows the anomalous Hall resistance R_{AHE} of BaM as a function of the in-plane magnetic field for positive and negative currents. As indicated by the grey arrows, the two loops evolve in entirely opposite manners. When a charge current is applied to the Pt film, the SOT breaks the symmetry of the magnetization orientation in response to the field, resulting in $\mathbf{M}_z \neq 0$. The symmetry is broken in a different manner for the charge currents of opposite signs, and this gives rise to the opposite evolutions shown in Figure 8.

The results above demonstrate the presence of a large SOT in HM/MI systems in comparison to HM/FM systems and the possibility of efficient SOT-induced switching in HM/MI systems, thereby presenting potential direction for the future development of magnetic memory and logic devices for energy-efficient computing. BaM was already used as recording media in magnetic tapes and hard drives [99,100]. Thus, future work includes developing BaM-based nanoscale elements for SOT-magnetic random access memory applications or doping BaM with scandium [101] to reduce the coercivity, replacing Pt with quantum materials that exhibit stronger spin-orbit coupling, such as topological insulators [7,102] that we will discuss in the next section.

3.3 Spin-Orbit Torque Switching in Topological Insulator/Hexagonal Ferrite Bilayers

Topological insulators (TIs) are expected to host spin-orbit coupling that is considerably stronger than in heavy metals and can thereby produce substantially larger SOT [103]. Recently, there have been a number of experimental demonstrations of SOT-induced magnetization switching in TI/FM bilayered structures [104–109]. The demonstrated switching efficiencies were all higher than in the heavy metal/FM counterparts, which provide substantial implications for future applications of TI materials. However, in those experiments, the FM films are all conductive, which shunted a significant amount of current; the topological insulators usually have a resistivity about one order of magnitude higher than FM. The direct consequence is that the charge current is not fully utilized to generate spin current. An even worse

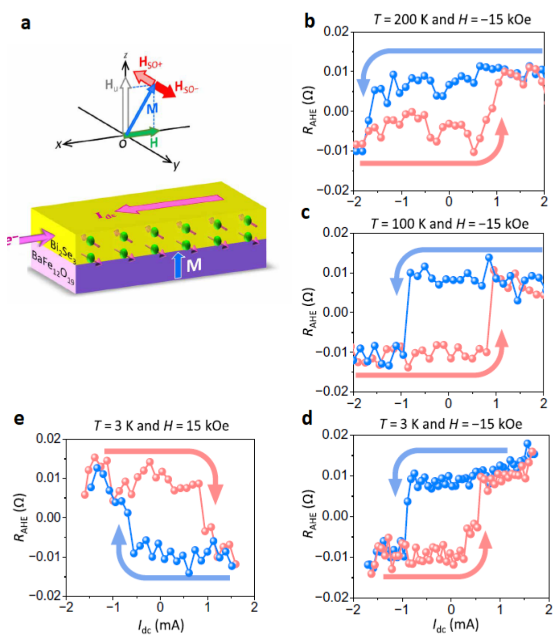

Figure 9. SOT-induced switching in $Bi_2Se_3/BaFe_{12}O_{19}$. (a) Schematics showing the $Bi_2Se_3/BaFe_{12}O_{19}$ sample, current (I_{dc}), magnetization (M), magnetic field (H) and spin-orbit torque effective fields (H_{SO+} and H_{SO-}). (B to E) AHE resistance (R_{AHE}) measured as a function of charge current (I_{dc}) at different fields (H) and temperatures (T), as indicated. The arrows in (B) to (E) indicate the current sweeping directions. Adapted from Ref. [112]. © The Authors, some rights reserved; exclusive licensee American Association for the Advancement of Science. Distributed under a Creative Commons Attribution NonCommercial License 4.0 (CC BY-NC) http://creativecommons.org/licenses/by-nc/4.0/

consequence is that the exotic topologic surface state (TSS), which accounts for the strong spin-orbit coupling, may be compromised because of the electrons' interactions from the neighboring FM layer. In fact, a number of theoretical works have suggested that significant modification or suppression can result from the coupling of a TI and FM [110–112]. Several experiments also provided experimental evidence to confirm the case: when a Fe layer is grown on a TI, the TSS bands disappeared [113]. This means that the strong SOTs measured in the TI/FM structures may not be explained by TSS fully.

In this regard, it is essential to study the SOT from *bona fide* TSS. A recent theoretical work compared the effects of conductive and insulating FM films on the TSSs in TI/FM heterostructures. It showed that, in stark contrast with the conductive FM case, the TSSs in a TI/magnetic insulator (MI) structure could be preserved mainly except for the opening of a small gap at the Dirac point when strong coupling exists at the interface [109].

In Ref. [114], the authors chose a Bi_2Se_3 (TI)/BaM (MI) heterostructure considering that both layers have the same hexagonal lattice structure to promote an epitaxial interface for spin transport [109]. It is found that the switching response in the BaM film strongly depends on the charge current applied to the TI film. As shown in Figure 9, when a constant magnetic field is applied in the film plane, the charge current in the TI film was strong enough to switch the magnetization in the BaM film up or down. When temperature decreased, the switching current reduced correspondingly. Figure 10 evidently indicates the presence of strong SOT responses at low T. The sharp increase of SOT below 100 K can be attributed to strong TSSs due to enhanced surface state conductivity and reduced magnon-phonon scattering. A Pt/BaM control sample further proved the strong SOT due to TSS in Bi_2Se_3/BaM.

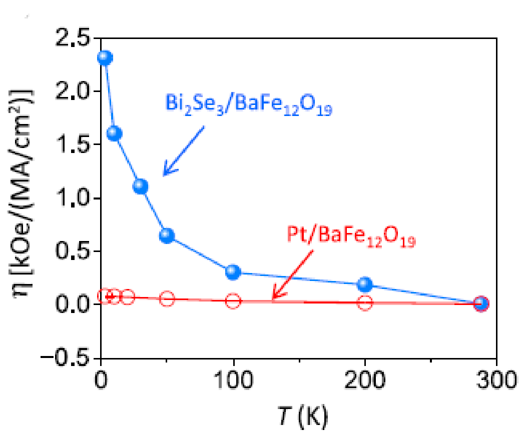

Figure 10. SOT efficiency (η) as a function of T in $Bi_2Se_3/BaFe_{12}O_{19}$ and $Pt/BaFe_{12}O_{19}$. In $Bi_2Se_3/BaFe_{12}O_{19}$, the rapid increase of η below 100 K demonstrates the impact of topological surface state on SOT. Adapted from Ref. [112].

Section 4. Outlook and Conclusion

Advances in the synthesis of magnetic insulator thin films have spurred new interests in spintronics, although it remains to be seen whether these materials will actually enable new classes of practical devices. For practical applications, fabrication processes should be developed to grow magnetic insulator thin films on Si substrates. A few studies have been devoted to addressing this issue. For example, pulsed laser deposition was used to deposit Ce:YIG thin films with a YIG seed layer on Si substrates [115]. Recently rare-earth garnets have been developed that crystallize on Si and quartz without a seed layer, including sputter-deposited terbium iron garnet (TIG) and Bi-doped TIG (Bi:TIG) [116–118]. Some of the efforts are focused on developing low-damping polycrystalline YIG thin films on Si substrates with ion beam sputtering and then annealing at elevated temperature [119]. Those efforts have laid the foundation for fabricating magnetic insulator thin films with physical vapor deposition techniques that could be compatible with the CMOS processes. It is conceivable that spinel ferrites, with a simpler structure and lower thermal budget for crystallization than garnets, are more suitable for ultimate integration with Si substrates. Further, whereas high-quality (e.g., low-damping) YIG thin films usually have an (111) orientation [30,120], recent demonstrations of (001)-oriented spinel ferrite thin films with low damping [44,53,79] suggest that they may be more accessible materials to be integrated with Si (001). The growth of high-quality epitaxial spinel ferrites on Si may be feasible if an appropriate nonmagnetic spinel seed layer is developed; this approach would be analogous to the growth of epitaxial perovskites on highly crystalline $SrTiO_3$ seed layers on Si [121]. While molecular beam epitaxy would enable the most precise control of film composition (which may be crucial for minimizing effective damping), recent experiments suggest that magnetron sputtering can be employed to grow reasonably low-damping coherent epitaxial ferrite thin films [122]. We also remark that standard patterning methods (e.g., photolithography or electron-beam lithography, followed by argon ion milling) are routinely used to fabricate devices based on epitaxial ferrite films. However, whether highly crystalline spinel ferrites with minimal defects – hence low effective damping or narrow FMR linewidths – can be realized while meeting the constraints of CMOS-compatible, high-throughput device production is an open question.

An alternative approach, which circumvents the need for crystalline films, is the use of *amorphous* magnetic insulators. Signatures of long-distance spin transport were reported in an amorphous magnetic insulator, which is both magnetically and structurally disordered [123]. Using amorphous insulator films that can be grown on virtually any substrates for spintronics is an intriguing prospect. However, some follow-up experiments indicate these reported signatures were actually due to parasitic leak currents, rather than spin transport [124]. Further studies are certainly required to understand spin dynamics and transport in amorphous magnetic insulators.

Another major hurdle against implementing magnetic insulators for practical applications is the lack of robust methods for reading the magnetization in the magnetic insulators. Through the HM/MI structure, the magnetization of the MI layer can be read by the spin Hall magnetoresistance [125–127], the anomalous Hall effect [128], or unidirectional magnetoresistance [129]. The typical magnetoresistance ratio is < 0.01%, which is too low for practical device applications. Some research works tried to explore the possibility of fabricating magnetic tunnel junctions with magnetic insulators and achieved tunneling magnetoresistance of 10% to 20% [130,131]. Still, more work is needed to amplify it to match the performance of a conductive magnet-based MTJ device. In addition, MTJ requires a modest resistance-area product, which can present significant challenges for magnetic insulator thin films with high resistances. Growing single-crystal magnetic insulators in a multilayer heterostructures are also challenging because different layers crystallize at different temperatures. In this regard, the spinel ferrite may be more practical for the integration in an MTJ due to its low crystallization temperature.

In conclusion, we have presented select recent studies and our perspectives on novel thin-film spinel ferrites and hexagonal ferrites. We believe that these ferrites are attractive alternatives to iron garnets that have dominated the rapidly growing field of insulator spintronics. With a simpler structure and lower crystallization temperature than garnets, spinel ferrites can be superior model systems and device platforms. The recent demonstrations of low damping in engineered epitaxial spinel ferrites [44,79] point to their promise as low-loss spintronic and magnonic media. Hexagonal ferrites possess strong perpendicular anisotropy of bulk origin, in comparison to iron garnets for which perpendicular anisotropy is of interfacial origin (strain-induced). The strong bulk anisotropy makes these hexaferrites convenient insulating media for probing perpendicular magnetic switching or domain wall motion driven by spin-orbit torques [98,114], along with potential applications requiring high thermal stability. Overall, further advances in the thin-film synthesis of spinel ferrites and hexaferrites will likely enable new fundamental insights into spin physics in insulators or across insulator/metal interfaces – and perhaps viable applications – beyond what is possible with iron garnets.

Data Availability Statement

The data that support the findings of this study are available from the corresponding author upon reasonable request.

Acknowledgements

Work by S.E. was supported in part by NSF Grant DMR-2003914.

References

1. A. Brataas, A. D. Kent, and H. Ohno, "Current-induced torques in magnetic materials.," Nat. Mater. **11**, 372–81 (2012).
2. D. C. Ralph and M. D. Stiles, "Spin transfer torques," J. Magn. Magn. Mater. **320**, 1190–1216 (2008).
3. C. Chappert, A. Fert, and F. N. Van Dau, "The emergence of spin electronics in data storage.," Nat. Mater. **6**, 813–23 (2007).
4. A. Hoffmann, "Spin Hall Effects in Metals," IEEE Trans. Magn. **49**, 5172–5193 (2013).
5. J. Sinova, S. O. Valenzuela, J. Wunderlich, C. H. Back, and T. Jungwirth, "Spin Hall effects," Rev. Mod. Phys. **87**, 1213–1260 (2015).
6. J. Li, G. Yu, C. Tang, Y. Liu, Z. Shi, Y. Liu, A. Navabi, M. Aldosary, Q. Shao, K. L. Wang, R. Lake, and J. Shi, "Deficiency of the bulk spin Hall effect model for spin-orbit torques in magnetic-insulator/heavy-metal heterostructures," Phys. Rev. B **95**, 241305 (2017).
7. A. R. Mellnik, J. S. Lee, A. Richardella, J. L. Grab, P. J. Mintun, M. H. Fischer, A. Vaezi, A. Manchon, E.-A. Kim, N. Samarth, and D. C. Ralph, "Spin-transfer torque generated by a topological insulator," Nature **511**, 449–451 (2014).
8. M. B. Jungfleisch, W. Zhang, J. Sklenar, W. Jiang, J. E. Pearson, J. B. Ketterson, and A. Hoffmann, "Interface-driven spin-torque ferromagnetic resonance by Rashba coupling at the interface between nonmagnetic materials," Phys. Rev. B **93**, 224419 (2016).
9. S. Emori, T. Nan, A. M. Belkessam, X. Wang, A. D. Matyushov, C. J. Babroski, Y. Gao, H. Lin, and N. X. Sun, "Interfacial spin-orbit torque without bulk spin-orbit coupling," Phys. Rev. B **93**, 180402 (2016).
10. A. Brataas and K. M. D. Hals, "Spin-orbit torques in action.," Nat. Nanotechnol. **9**, 86–8 (2014).
11. A. V. Chumak, V. I. Vasyuchka, A. A. Serga, and B. Hillebrands, "Magnon spintronics," Nat. Phys. **11**, 453–461 (2015).
12. S. O. Demokritov and A. N. Slavin, eds., *Magnonics: From Fundamentals to Applications* (Springer Berlin Heidelberg, 2012).
13. A. Hoffmann and S. D. Bader, "Opportunities at the Frontiers of Spintronics," Phys. Rev. Appl. **4**, 47001 (2015).
14. A. Azevedo, L. H. Vilela-Leão, R. L. Rodríguez-Suárez, A. F. Lacerda Santos, and S. M. Rezende, "Spin pumping and anisotropic magnetoresistance voltages in magnetic bilayers: Theory and experiment," Phys. Rev. B **83**, 144402 (2011).
15. L. Bai, P. Hyde, Y. S. Gui, C.-M. Hu, V. Vlaminck, J. E. Pearson, S. D. Bader, and A. Hoffmann,

"Universal Method for Separating Spin Pumping from Spin Rectification Voltage of Ferromagnetic Resonance," Phys. Rev. Lett. **111**, 217602 (2013).

16. M. Obstbaum, M. Härtinger, H. G. Bauer, T. Meier, F. Swientek, C. H. Back, and G. Woltersdorf, "Inverse spin Hall effect in $Ni_{81}Fe_{19}$/normal-metal bilayers," Phys. Rev. B **89**, 60407 (2014).
17. R. Iguchi and E. Saitoh, "Measurement of Spin Pumping Voltage Separated from Extrinsic Microwave Effects," J. Phys. Soc. Japan **86**, 11003 (2017).
18. W. Wang, T. Wang, V. P. Amin, Y. Wang, A. Radhakrishnan, A. Davidson, S. R. Allen, T. J. Silva, H. Ohldag, D. Balzar, B. L. Zink, P. M. Haney, J. Q. Xiao, D. G. Cahill, V. O. Lorenz, and X. Fan, "Anomalous spin–orbit torques in magnetic single-layer films," Nat. Nanotechnol. **14**, 819–824 (2019).
19. V. P. Amin, J. Li, M. D. Stiles, and P. M. Haney, "Intrinsic spin currents in ferromagnets," Phys. Rev. B **99**, 220405 (2019).
20. C. Du, H. Wang, P. C. Hammel, and F. Yang, "$Y_3Fe_5O_{12}$ spin pumping for quantitative understanding of pure spin transport and spin Hall effect in a broad range of materials," J. Appl. Phys. **117**, 172603 (2015).
21. C. O. Avci, A. Quindeau, C.-F. Pai, M. Mann, L. Caretta, A. S. Tang, M. C. Onbasli, C. A. Ross, and G. S. D. Beach, "Current-induced switching in a magnetic insulator," Nat. Mater. **16**, 309 (2017).
22. L. Soumah, N. Beaulieu, L. Qassym, C. Carrétéro, E. Jacquet, R. Lebourgeois, J. Ben Youssef, P. Bortolotti, V. Cros, and A. Anane, "Ultra-low damping insulating magnetic thin films get perpendicular," Nat. Commun. **9**, 3355 (2018).
23. C. O. Avci, E. Rosenberg, L. Caretta, F. Büttner, M. Mann, C. Marcus, D. Bono, C. A. Ross, and G. S. D. Beach, "Interface-driven chiral magnetism and current-driven domain walls in insulating magnetic garnets," Nat. Nanotechnol. **14**, 561 (2019).
24. B. Heinrich, "Spin Relaxation in Magnetic Metallic Layers and Multilayers," in *Ultrathin Magnetic Structures III*, J. A. C. Bland and B. Heinrich, eds. (Springer-Verlag, 2005), pp. 143–210.
25. C. K. A. Mewes and T. Mewes, "Relaxation in Magnetic Materials for Spintronics," in *Handbook of Nanomagnetism: Applications and Tools* (Pan Stanford, 2015), pp. 71–95.
26. V. G. Harris, "Modern Microwave Ferrites," IEEE Trans. Magn. **48**, 1075–1104 (2012).
27. M. Pardavi-Horvath, "Microwave applications of soft ferrites," J. Magn. Magn. Mater. **215**–**216**, 171–183 (2000).
28. R. C. LeCraw, E. G. Spencer, and C. S. Porter, "Ferromagnetic resonance line width in yttrium iron garnet single crystals," Phys. Rev. **110**, 1311–1313 (1958).

29. B. M. Howe, S. Emori, H.-M. Jeon, T. M. Oxholm, J. G. Jones, K. Mahalingam, Y. Zhuang, N. X. Sun, and G. J. Brown, "Pseudomorphic Yttrium Iron Garnet Thin Films With Low Damping and Inhomogeneous Linewidth Broadening," IEEE Magn. Lett. **6**, 3500504 (2015).
30. H. Chang, P. Li, W. Zhang, T. Liu, A. Hoffmann, L. Deng, and M. Wu, "Nanometer-Thick Yttrium Iron Garnet Films With Extremely Low Damping," IEEE Magn. Lett. **5**, 1–4 (2014).
31. O. d'Allivy Kelly, A. Anane, R. Bernard, J. Ben Youssef, C. Hahn, A. H. Molpeceres, C. Carrétéro, E. Jacquet, C. Deranlot, P. Bortolotti, R. Lebourgeois, J.-C. Mage, G. de Loubens, O. Klein, V. Cros, and A. Fert, "Inverse spin Hall effect in nanometer-thick yttrium iron garnet/Pt system," Appl. Phys. Lett. **103**, 82408 (2013).
32. C. Tang, M. Aldosary, Z. Jiang, H. Chang, B. Madon, K. Chan, M. Wu, J. E. Garay, and J. Shi, "Exquisite growth control and magnetic properties of yttrium iron garnet thin films," Appl. Phys. Lett. **108**, 102403 (2016).
33. J. Lustikova, Y. Shiomi, Z. Qiu, T. Kikkawa, R. Iguchi, K. Uchida, and E. Saitoh, "Spin current generation from sputtered Y3Fe5O12 films," J. Appl. Phys. **116**, 153902 (2014).
34. M. C. Onbasli, A. Kehlberger, D. H. Kim, G. Jakob, M. Kläui, A. V. Chumak, B. Hillebrands, and C. A. Ross, "Pulsed laser deposition of epitaxial yttrium iron garnet films with low Gilbert damping and bulk-like magnetization," APL Mater. **2**, 106102 (2014).
35. C. Hauser, T. Richter, N. Homonnay, C. Eisenschmidt, M. Qaid, H. Deniz, D. Hesse, M. Sawicki, S. G. Ebbinghaus, and G. Schmidt, "Yttrium Iron Garnet Thin Films with Very Low Damping Obtained by Recrystallization of Amorphous Material," Sci. Rep. **6**, 20827 (2016).
36. A. Talalaevskij, M. Decker, J. Stigloher, A. Mitra, H. S. Körner, O. Cespedes, C. H. Back, and B. J. Hickey, "Magnetic properties of spin waves in thin yttrium iron garnet films," Phys. Rev. B **95**, 64409 (2017).
37. M. Weiler, M. Althammer, M. Schreier, J. Lotze, M. Pernpeintner, S. Meyer, H. Huebl, R. Gross, A. Kamra, J. Xiao, Y.-T. Chen, H. Jiao, G. E. W. Bauer, and S. T. B. Goennenwein, "Experimental Test of the Spin Mixing Interface Conductivity Concept," Phys. Rev. Lett. **111**, 176601 (2013).
38. F.-J. Chang, J. G. Lin, and S.-Y. Huang, "Robust spin current generated by the spin Seebeck effect," Phys. Rev. Mater. **1**, 31401 (2017).
39. M. B. Jungfleisch, W. Zhang, J. Sklenar, J. Ding, W. Jiang, H. Chang, F. Y. Fradin, J. E. Pearson, J. B. Ketterson, V. Novosad, M. Wu, and A. Hoffmann, "Large Spin-Wave Bullet in a Ferrimagnetic Insulator Driven by the Spin Hall Effect," Phys. Rev. Lett. **116**, 57601 (2016).
40. M. Collet, X. de Milly, O. d'Allivy Kelly, V. V. Naletov, R. Bernard, P. Bortolotti, J. Ben Youssef, V. E. Demidov, S. O. Demokritov, J. L. Prieto, M. Muñoz, V. Cros, A. Anane, G. de

Loubens, and O. Klein, "Generation of coherent spin-wave modes in yttrium iron garnet microdiscs by spin–orbit torque," Nat. Commun. **7**, 10377 (2016).

41. C. Safranski, I. Barsukov, H. K. Lee, T. Schneider, A. A. Jara, A. Smith, H. Chang, K. Lenz, J. Lindner, Y. Tserkovnyak, M. Wu, and I. N. Krivorotov, "Spin caloritronic nano-oscillator," Nat. Commun. **8**, 117 (2017).
42. S. Emori, A. Matyushov, H.-M. Jeon, C. J. Babroski, T. Nan, A. M. Belkessam, J. G. Jones, M. E. McConney, G. J. Brown, B. M. Howe, and N. X. Sun, "Spin-orbit torque and spin pumping in YIG/Pt with interfacial insertion layers," Appl. Phys. Lett. **112**, 182406 (2018).
43. W.-H. Hsu and R. H. Victora, "Spin–Orbit Torque Switching in Low-Damping Magnetic Insulators: A Micrmomagnetic Study," IEEE Magn. Lett. **11**, 1–5 (2020).
44. S. Emori, D. Yi, S. Crossley, J. J. Wisser, P. P. Balakrishnan, P. Shafer, C. Klewe, A. T. N'Diaye, B. T. Urwin, K. Mahalingam, B. M. Howe, H. Y. Hwang, E. Arenholz, and Y. Suzuki, "Ultralow Damping in Nanometer-Thick Epitaxial Spinel Ferrite Thin Films," Nano Lett. **18**, 4273–4278 (2018).
45. L. J. Riddiford, J. J. Wisser, S. Emori, P. Li, D. Roy, E. Cogulu, O. van 't Erve, Y. Deng, S. X. Wang, B. T. Jonker, A. D. Kent, and Y. Suzuki, "Efficient spin current generation in low-damping $Mg(Al, Fe)_2O_4$ thin films," Appl. Phys. Lett. **115**, 122401 (2019).
46. P. Li, L. J. Riddiford, C. Bi, J. J. Wisser, X.-Q. Sun, A. Vailionis, M. J. Veit, A. Altman, X. Li, M. DC, S. X. Wang, Y. Suzuki, and S. Emori, "Giant Internal Spin-Hall Ratio of Order Unity in Highly Crystalline Pt," arXiv:2009.04894 (2020).
47. M. Wu, "M-Type Barium Hexagonal Ferrite Films," in *Advanced Magnetic Materials* (InTech, 2012).
48. Y. Suzuki, "Epitaxial Spinel Ferrite Thin Films," Annu. Rev. Mater. Res. **31**, 265–289 (2001).
49. A. K. Srivastava, M. J. Hurben, M. A. Wittenauer, P. Kabos, C. E. Patton, R. Ramesh, P. C. Dorsey, and D. B. Chrisey, "Angle dependence of the ferromagnetic resonance linewidth and two magnon losses in pulsed laser deposited films of yttrium iron garnet, MnZn ferrite, and NiZn ferrite," J. Appl. Phys. **85**, 7838 (1999).
50. D. Roy, S. Sakshath, G. Singh, R. Joshi, S V Bhat, and P. S. Anil Kumar, "Investigation on two magnon scattering processes in pulsed laser deposited epitaxial nickel zinc ferrite thin film," J. Phys. D. Appl. Phys. **48**, 125004 (2015).
51. R. Datta, S. Kanuri, S. V. Karthik, D. Mazumdar, J. X. Ma, and A. Gupta, "Formation of antiphase domains in $NiFe_2O_4$ thin films deposited on different substrates," Appl. Phys. Lett. **97**, 71907 (2010).
52. N. Pachauri, B. Khodadadi, A. V. Singh, J. B. Mohammadi, R. L. Martens, P. R. LeClair, C.

Mewes, T. Mewes, and A. Gupta, "A comprehensive study of ferromagnetic resonance and structural properties of iron-rich nickel ferrite ($Ni_xFe_{3-x}O_4$, x≤1) films grown by chemical vapor deposition," J. Magn. Magn. Mater. **417**, 137–142 (2016).

53. A. V. Singh, B. Khodadadi, J. B. Mohammadi, S. Keshavarz, T. Mewes, D. S. Negi, R. Datta, Z. Galazka, R. Uecker, and A. Gupta, "Bulk Single Crystal-Like Structural and Magnetic Characteristics of Epitaxial Spinel Ferrite Thin Films with Elimination of Antiphase Boundaries," Adv. Mater. **29**, 1701222 (2017).

54. X. Liu, C.-F. Chang, A. D. Rata, A. C. Komarek, and L. H. Tjeng, "Fe_3O_4 thin films: controlling and manipulating an elusive quantum material," npj Quantum Mater. **1**, 16027 (2016).

55. R. Arias and D. L. Mills, "Extrinsic contributions to the ferromagnetic resonance response of ultrathin films," Phys. Rev. B **60**, 7395–7409 (1999).

56. R. D. McMichael and P. Krivosik, "Classical Model of Extrinsic Ferromagnetic Resonance Linewidth in Ultrathin Films," IEEE Trans. Magn. **40**, 2–11 (2004).

57. S. Emori, B. A. Gray, H.-M. Jeon, J. Peoples, M. Schmitt, K. Mahalingam, M. Hill, M. E. Mcconney, M. T. Gray, U. S. Alaan, A. C. Bornstein, P. Shafer, A. T. N'Diaye, E. Arenholz, G. Haugstad, K.-Y. Meng, F. Yang, D. Li, S. Mahat, D. G. Cahill, P. Dhagat, A. Jander, N. X. Sun, Y. Suzuki, and B. M. Howe, "Coexistence of Low Damping and Strong Magnetoelastic Coupling in Epitaxial Spinel Ferrite Thin Films," Adv. Mater. **29**, 1701130 (2017).

58. R. C. Budhani, S. Emori, Z. Galazka, B. A. Gray, M. Schmitt, J. J. Wisser, H. M. Jeon, H. Smith, P. Shah, M. R. Page, M. E. McConney, Y. Suzuki, and B. M. Howe, "Pseudomorphic spinel ferrite films with perpendicular anisotropy and low damping," Appl. Phys. Lett. **113**, 82404 (2018).

59. S. Geprägs, A. Kehlberger, F. Della Coletta, Z. Qiu, E.-J. Guo, T. Schulz, C. Mix, S. Meyer, A. Kamra, M. Althammer, H. Huebl, G. Jakob, Y. Ohnuma, H. Adachi, J. Barker, S. Maekawa, G. E. W. Bauer, E. Saitoh, R. Gross, S. T. B. Goennenwein, and M. Kläui, "Origin of the spin Seebeck effect in compensated ferrimagnets," Nat. Commun. **7**, 10452 (2016).

60. K. Ganzhorn, J. Barker, R. Schlitz, B. A. Piot, K. Ollefs, F. Guillou, F. Wilhelm, A. Rogalev, M. Opel, M. Althammer, S. Geprägs, H. Huebl, R. Gross, G. E. W. Bauer, and S. T. B. Goennenwein, "Spin Hall magnetoresistance in a canted ferrimagnet," Phys. Rev. B **94**, 94401 (2016).

61. J. J. Wisser, S. Emori, L. Riddiford, A. Altman, P. Li, K. Mahalingam, B. T. Urwin, B. M. Howe, M. R. Page, A. J. Grutter, B. J. Kirby, and Y. Suzuki, "Ultrathin interfacial layer with suppressed room temperature magnetization in magnesium aluminum ferrite thin films," Appl. Phys. Lett. **115**, 132404 (2019).

62. J. J. Wisser, A. J. Grutter, D. A. Gilbert, A. T. N'Diaye, C. Klewe, P. Shafer, E. Arenholz, Y. Suzuki, and S. Emori, "Damping Enhancement in Coherent Ferrite–Insulating-Paramagnet

Bilayers," Phys. Rev. Appl. **12**, 54044 (2019).
63. A. Mitra, O. Cespedes, Q. Ramasse, M. Ali, S. Marmion, M. Ward, R. M. D. Brydson, C. J. Kinane, J. F. K. Cooper, S. Langridge, and B. J. Hickey, "Interfacial Origin of the Magnetisation Suppression of Thin Film Yttrium Iron Garnet," Sci. Rep. **7**, 11774 (2017).
64. J. F. K. Cooper, C. J. Kinane, S. Langridge, M. Ali, B. J. Hickey, T. Niizeki, K. Uchida, E. Saitoh, H. Ambaye, and A. Glavic, "Unexpected structural and magnetic depth dependence of YIG thin films," Phys. Rev. B **96**, 104404 (2017).
65. A. J. Lee, A. S. Ahmed, S. Guo, B. D. Esser, D. W. McComb, and F. Yang, "Epitaxial Co 50 Fe 50 (110)/Pt(111) films on $MgAl_2O_4$ (001) and its enhancement of perpendicular magnetic anisotropy," J. Appl. Phys. **125**, 183903 (2019).
66. A. J. Lee, J. T. Brangham, Y. Cheng, S. P. White, W. T. Ruane, B. D. Esser, D. W. McComb, P. C. Hammel, and F. Yang, "Metallic ferromagnetic films with magnetic damping under 1.4×10^{-3}," Nat. Commun. **8**, 234 (2017).
67. B. Khodadadi, A. Rai, A. Sapkota, A. Srivastava, B. Nepal, Y. Lim, D. A. Smith, C. Mewes, S. Budhathoki, A. J. Hauser, M. Gao, J.-F. Li, D. D. Viehland, Z. Jiang, J. J. Heremans, P. V. Balachandran, T. Mewes, and S. Emori, "Conductivitylike Gilbert Damping due to Intraband Scattering in Epitaxial Iron," Phys. Rev. Lett. **124**, 157201 (2020).
68. J. J. Krebs, D. M. Lind, and S. D. Berry, "Ferromagnetic resonance and spin anisotropy in iron oxide thin films and iron oxide/nickel oxide superlattices," J. Appl. Phys. **73**, 6457–6459 (1993).
69. J. A. Borchers, R. W. Erwin, S. D. Berry, D. M. Lind, J. F. Ankner, E. Lochner, K. A. Shaw, and D. Hilton, "Long-range magnetic order in Fe_3O_4/NiO superlattices," Phys. Rev. B **51**, 8276–8286 (1995).
70. W. Niu, Y. Zhang, Y. Gan, D. V. Christensen, M. V. Soosten, E. J. Garcia-Suarez, A. Riisager, X. Wang, Y. Xu, R. Zhang, N. Pryds, and Y. Chen, "Giant Tunability of the Two-Dimensional Electron Gas at the Interface of γ-Al_2O_3/$SrTiO_3$," Nano Lett. **17**, 6878–6885 (2017).
71. J. Ding, J. Cheng, F. Dogan, Y. Li, W. Lin, Y. Yao, A. Manchon, K. Yang, and T. Wu, "Two-Dimensional Electron Gas at Spinel/Perovskite Interface: Suppression of Polar Catastrophe by an Ultrathin Layer of Interfacial Defects," ACS Appl. Mater. Interfaces 12, 42982 (2020).
72. H. S. Körner, M. A. W. Schoen, T. Mayer, M. M. Decker, J. Stigloher, T. Weindler, T. N. G. Meier, M. Kronseder, and C. H. Back, "Magnetic damping in poly-crystalline $Co_{25}Fe_{75}$: Ferromagnetic resonance vs. spin wave propagation experiments," Appl. Phys. Lett. **111**, 132406 (2017).
73. H. L. Wang, C. H. Du, Y. Pu, R. Adur, P. C. Hammel, and F. Y. Yang, "Scaling of Spin Hall Angle in 3d, 4d, and 5d Metals from $Y_3Fe_5O_{12}$/Metal Spin Pumping," Phys. Rev. Lett. **112**,

197201 (2014).

74. J. J. Wisser, L. J. Riddiford, A. Altman, P. Li, S. Emori, P. Shafer, C. Klewe, A. T. N'Diaye, E. Arenholz, and Y. Suzuki, "The role of iron in magnetic damping of $Mg(Al,Fe)_2O_4$ spinel ferrite thin films," Appl. Phys. Lett. **116**, 142406 (2020).

75. G. F. Dionne, "The Magnetoelastic Ion: Friend and Foe to Microwaves," IEEE Trans. Magn. **47**, 272–278 (2011).

76. N. Pachauri, B. Khodadadi, M. Althammer, A. V. Singh, B. Loukya, R. Datta, M. Iliev, L. Bezmaternykh, I. Gudim, T. Mewes, and A. Gupta, "Study of structural and ferromagnetic resonance properties of spinel lithium ferrite ($LiFe_5O_8$) single crystals," J. Appl. Phys. **117**, 233907 (2015).

77. U. S. Alaan, G. Sreenivasulu, K. M. Yu, C. Jenkins, P. Shafer, E. Arenholz, G. Srinivasan, and Y. Suzuki, "Controlling disorder-mediated exchange bias in $(Mn,Zn,Fe)_3O_4$ thin films," J. Magn. Magn. Mater. **405**, 129–136 (2016).

78. L. Zhu, D. C. Ralph, and R. A. Buhrman, "Effective Spin-Mixing Conductance of Heavy-Metal–Ferromagnet Interfaces," Phys. Rev. Lett. **123**, 57203 (2019).

79. X. Y. Zheng, L. J. Riddiford, J. J. Wisser, S. Emori, and Y. Suzuki, "Ultra-low magnetic damping in epitaxial $Li_{0.5}Fe_{2.5}O_4$ thin films," Appl. Phys. Lett. **117**, 92407 (2020).

80. L. Liu, T. Moriyama, D. C. Ralph, and R. A. Buhrman, "Spin-Torque Ferromagnetic Resonance Induced by the Spin Hall Effect," Phys. Rev. Lett. **106**, 36601 (2011).

81. T. Nan, S. Emori, C. T. Boone, X. Wang, T. M. Oxholm, J. G. Jones, B. M. Howe, G. J. Brown, and N. X. Sun, "Comparison of spin-orbit torques and spin pumping across NiFe/Pt and NiFe/Cu/Pt interfaces," Phys. Rev. B **91**, 214416 (2015).

82. M. T. Gray, S. Emori, B. A. Gray, H. Jeon, O. M. J. van 't Erve, B. T. Jonker, S. Kim, M. Suzuki, T. Ono, B. M. Howe, and Y. Suzuki, "Spin-Current Generation in Low-Damping $Ni_{0.65}Zn_{0.35}Al_{0.8}Fe_{1.2}O_4$ Spinel Ferrite," Phys. Rev. Appl. **9**, 64039 (2018).

83. Y. Li, T. Polakovic, Y.-L. Wang, J. Xu, S. Lendinez, Z. Zhang, J. Ding, T. Khaire, H. Saglam, R. Divan, J. Pearson, W.-K. Kwok, Z. Xiao, V. Novosad, A. Hoffmann, and W. Zhang, "Strong Coupling between Magnons and Microwave Photons in On-Chip Ferromagnet-Superconductor Thin-Film Devices," Phys. Rev. Lett. **123**, 107701 (2019).

84. H. Wang, C. Du, P. C. Hammel, and F. Yang, "Antiferromagnonic spin transport from $Y_3Fe_5O_{12}$ into NiO.," Phys. Rev. Lett. **113**, 97202 (2014).

85. W. Lin, K. Chen, S. Zhang, and C. L. Chien, "Enhancement of Thermally Injected Spin Current through an Antiferromagnetic Insulator," Phys. Rev. Lett. **116**, 186601 (2016).

86. Q. Li, M. Yang, C. Klewe, P. Shafer, A. T. N'Diaye, D. Hou, T. Y. Wang, N. Gao, E. Saitoh, C.

Hwang, R. J. Hicken, J. Li, E. Arenholz, and Z. Q. Qiu, "Coherent ac spin current transmission across an antiferromagnetic CoO insulator," Nat. Commun. **10**, 5265 (2019).

87. J. Finley and L. Liu, "Spintronics with compensated ferrimagnets," Appl. Phys. Lett. **116**, 110501 (2020).

88. T. R. McGuire, "Microwave Resonance Absorption in Nickel Ferrite-Aluminate," Phys. Rev. **93**, 682–686 (1954).

89. M. Shalaby, F. Vidal, M. Peccianti, R. Morandotti, F. Enderli, T. Feurer, and B. D. Patterson, "Terahertz macrospin dynamics in insulating ferrimagnets," Phys. Rev. B **88**, 140301 (2013).

90. L. Liensberger, A. Kamra, H. Maier-Flaig, S. Geprägs, A. Erb, S. T. B. Goennenwein, R. Gross, W. Belzig, H. Huebl, and M. Weiler, "Exchange-enhanced ultrastrong magnon-magnon coupling in a compensated ferrimagnet," Phys. Rev. Lett. **123**, 117204 (2019).

91. L. Alahmed and P. Li, "Perpendicular Magnetic Insulator Films for Spintronics," in *Magnetic Materials [Working Title]* (IntechOpen, 2020).

92. W. H. Von Aulock, *Handbook of Microwave Ferrite Materials* (Academic Press, 1965).

93. R. C. Pullar, "Hexagonal ferrites: A review of the synthesis, properties and applications of hexaferrite ceramics," Prog. Mater. Sci. **57**, 1191–1334 (2012).

94. S. Ikeda, K. Miura, H. Yamamoto, K. Mizunuma, H. D. Gan, M. Endo, S. Kanai, J. Hayakawa, F. Matsukura, and H. Ohno, "A perpendicular-anisotropy CoFeB-MgO magnetic tunnel junction," Nat. Mater. **9**, 721–724 (2010).

95. L. Liu, C.-F. Pai, Y. Li, H. W. Tseng, D. C. Ralph, and R. A. Buhrman, "Spin-torque switching with the giant spin Hall effect of tantalum.," Science **336**, 555–8 (2012).

96. S. Emori, U. Bauer, S.-M. Ahn, E. Martinez, and G. S. D. Beach, "Current-driven dynamics of chiral ferromagnetic domain walls.," Nat. Mater. **12**, 611–6 (2013).

97. W. Zhang, W. Han, X. Jiang, S.-H. Yang, and S. S. P. Parkin, "Role of transparency of platinum–ferromagnet interfaces in determining the intrinsic magnitude of the spin Hall effect," Nat. Phys. **11**, 496 (2015).

98. P. Li, T. Liu, H. Chang, A. Kalitsov, W. Zhang, G. Csaba, W. Li, D. Richardson, A. DeMann, G. Rimal, H. Dey, J. S. Jiang, W. Porod, S. B. Field, J. Tang, M. C. Marconi, A. Hoffmann, O. Mryasov, and M. Wu, "Spin–orbit torque-assisted switching in magnetic insulator thin films with perpendicular magnetic anisotropy," Nat. Commun. **7**, 12688 (2016).

99. T. Harasawa, R. Suzuki, O. Shimizu, S. Olcer, and E. Eleftheriou, "Barium-Ferrite particulate media for high-recording-density tape storage systems," in *IEEE Transactions on Magnetics* (2010), Vol. 46, pp. 1894–1897.

100. B. Zhou, B. S. D. C. S. Varaprasad, Z. Dai, D. E. Laughlin, and J. G. Zhu, "The effect of adding a

magnetic oxide in the grain boundaries of HAMR media," Appl. Phys. Lett. **113**, 82401 (2018).

101. X. Zuo, P. Shi, S. A. Oliver, and C. Vittoria, "Single crystal hexaferrite phase shifter at Ka band," J. Appl. Phys. **91**, 7622–7624 (2002).

102. Y. Fan, P. Upadhyaya, X. Kou, M. Lang, S. Takei, Z. Wang, J. Tang, L. He, L.-T. Chang, M. Montazeri, G. Yu, W. Jiang, T. Nie, R. N. Schwartz, Y. Tserkovnyak, and K. L. Wang, "Magnetization switching through giant spin–orbit torque in a magnetically doped topological insulator heterostructure," Nat. Mater. **13**, 699–704 (2014).

103. X. L. Qi and S. C. Zhang, "Topological insulators and superconductors," Rev. Mod. Phys. **83**, 1057 (2011).

104. J. Han, A. Richardella, S. A. Siddiqui, J. Finley, N. Samarth, and L. Liu, "Room-Temperature Spin-Orbit Torque Switching Induced by a Topological Insulator," Phys. Rev. Lett. **119**, 77702 (2017).

105. Y. Wang, D. Zhu, Y. Wu, Y. Yang, J. Yu, R. Ramaswamy, R. Mishra, S. Shi, M. Elyasi, K.-L. Teo, Y. Wu, and H. Yang, "Room temperature magnetization switching in topological insulator-ferromagnet heterostructures by spin-orbit torques," Nat. Commun. **8**, 1364 (2017).

106. M. DC, R. Grassi, J.-Y. Chen, M. Jamali, D. Reifsnyder Hickey, D. Zhang, Z. Zhao, H. Li, P. Quarterman, Y. Lv, M. Li, A. Manchon, K. A. Mkhoyan, T. Low, and J.-P. Wang, "Room-temperature high spin–orbit torque due to quantum confinement in sputtered $Bi_xSe_{(1-x)}$ films," Nat. Mater. **17**, 800–807 (2018).

107. K. Yasuda, A. Tsukazaki, R. Yoshimi, K. Kondou, K. S. Takahashi, Y. Otani, M. Kawasaki, and Y. Tokura, "Current-Nonlinear Hall Effect and Spin-Orbit Torque Magnetization Switching in a Magnetic Topological Insulator," Phys. Rev. Lett. **119**, 137204 (2017).

108. N. H. D. Khang, Y. Ueda, and P. N. Hai, "A conductive topological insulator with large spin Hall effect for ultralow power spin–orbit torque switching," Nat. Mater. **17**, 808–813 (2018).

109. Y. Li, Q. Ma, S. X. Huang, and C. L. Chien, "Thin films of topological kondo insulator candidate SmB6: Strong spin-orbit torque without exclusive surface conduction," Sci. Adv. **4**, eaap8294 (2018).

110. L. A. Wray, S. Y. Xu, Y. Xia, D. Hsieh, A. V. Fedorov, Y. S. Hor, R. J. Cava, A. Bansil, H. Lin, and M. Z. Hasan, "A topological insulator surface under strong Coulomb, magnetic and disorder perturbations," Nat. Phys. **7**, 32–37 (2011).

111. J. M. Marmolejo-Tejada, K. Dolui, P. Lazić, P.-H. Chang, S. Smidstrup, D. Stradi, K. Stokbro, and B. K. Nikolić, "Proximity Band Structure and Spin Textures on Both Sides of Topological-Insulator/Ferromagnetic-Metal Interface and Their Charge Transport Probes," Nano Lett. **17**, 5626–5633 (2017).

112. J. Zhang, J. P. Velev, X. Dang, and E. Y. Tsymbal, "Band structure and spin texture of Bi 2 Se 3 3 d ferromagnetic metal interface," Phys. Rev. B **94**, 14435 (2016).

113. J.-C. Rojas-Sánchez, S. Oyarzún, Y. Fu, A. Marty, C. Vergnaud, S. Gambarelli, L. Vila, M. Jamet, Y. Ohtsubo, A. Taleb-Ibrahimi, P. Le Fèvre, F. Bertran, N. Reyren, J.-M. George, and A. Fert, "Spin to Charge Conversion at Room Temperature by Spin Pumping into a New Type of Topological Insulator: α -Sn Films," Phys. Rev. Lett. **116**, 96602 (2016).

114. P. Li, J. Kally, S. S.-L. Zhang, T. Pillsbury, J. Ding, G. Csaba, J. Ding, J. S. Jiang, Y. Liu, R. Sinclair, C. Bi, A. DeMann, G. Rimal, W. Zhang, S. B. Field, J. Tang, W. Wang, O. G. Heinonen, V. Novosad, A. Hoffmann, N. Samarth, and M. Wu, "Magnetization switching using topological surface states," Sci. Adv. **5**, eaaw3415 (2019).

115. L. Bi, J. Hu, P. Jiang, D. H. Kim, G. F. Dionne, L. C. Kimerling, and C. A. Ross, "On-chip optical isolation in monolithically integrated non-reciprocal optical resonators," Nat. Photonics **5**, 758–762 (2011).

116. P. Dulal, A. D. Block, T. E. Gage, H. A. Haldren, S. Y. Sung, D. C. Hutchings, and B. J. H. Stadler, "Optimized Magneto-optical Isolator Designs Inspired by Seedlayer-Free Terbium Iron Garnets with Opposite Chirality," ACS Photonics **3**, 1818–1825 (2016).

117. C. Zhang, P. Dulal, B. J. H. Stadler, and D. C. Hutchings, "Monolithically-Integrated TE-mode 1D Silicon-on-Insulator Isolators using Seedlayer-Free Garnet," Sci. Rep. **7**, 1–8 (2017).

118. T. Fakhrul, S. Tazlaru, L. Beran, Y. Zhang, M. Veis, and C. A. Ross, "Magneto-Optical Bi:YIG Films with High Figure of Merit for Nonreciprocal Photonics," Adv. Opt. Mater. **7**, 1900056 (2019).

119. A. I. Stognij, N. N. Novitskii, O. L. Golikova, A. V. Bespalov, R. Gieniusz, A. Maziewski, A. Stupakiewicz, M. N. Smirnova, and V. A. Ketsko, "Growth of $Y_3Fe_5O_{12}$ films on Si with AlO_x and SiO_2 buffer layers by ion beam sputtering," Inorg. Mater. **53**, 1069–1074 (2017).

120. J. Ding, C. Liu, Y. Zhang, U. Erugu, Z. Quan, R. Yu, E. McCollum, S. Mo, S. Yang, H. Ding, X. Xu, J. Tang, X. Yang, and M. Wu, "Nanometer-Thick Yttrium Iron Garnet Films with Perpendicular Anisotropy and Low Damping," Phys. Rev. Appl. **14**, 14017 (2020).

121. S. A. Chambers, Y. Liang, Z. Yu, R. Droopad, J. Ramdani, and K. Eisenbeiser, "Band discontinuities at epitaxial $SrTiO_3$/Si(001) heterojunctions," Appl. Phys. Lett. **77**, 1662–1664 (2000).

122. J. Lumetzberger, M. Buchner, S. Pile, V. Ney, W. Gaderbauer, N. Daffé, M. V. Moro, D. Primetzhofer, K. Lenz, and A. Ney, "Influence of structure and cation distribution on magnetic anisotropy and damping in Zn/Al doped nickel ferrites," Phys. Rev. B **102**, 54402 (2020).

123. D. Wesenberg, T. Liu, D. Balzar, M. Wu, and B. L. Zink, "Long-distance spin transport in a

disordered magnetic insulator," Nat. Phys. **13**, 987–993 (2017).

124. J. M. Gomez-Perez, K. Oyanagi, R. Yahiro, R. Ramos, L. E. Hueso, E. Saitoh, and F. Casanova, "Absence of evidence of spin transport through amorphous $Y_3Fe_5O_{12}$," Appl. Phys. Lett. **116**, 32401 (2020).

125. H. Nakayama, M. Althammer, Y.-T. Chen, K. Uchida, Y. Kajiwara, D. Kikuchi, T. Ohtani, S. Geprägs, M. Opel, S. Takahashi, R. Gross, G. E. W. Bauer, S. T. B. Goennenwein, and E. Saitoh, "Spin Hall Magnetoresistance Induced by a Nonequilibrium Proximity Effect," Phys. Rev. Lett. **110**, 206601 (2013).

126. M. Althammer, S. Meyer, H. Nakayama, M. Schreier, S. Altmannshofer, M. Weiler, H. Huebl, S. Geprägs, M. Opel, R. Gross, D. Meier, C. Klewe, T. Kuschel, J.-M. Schmalhorst, G. Reiss, L. Shen, A. Gupta, Y.-T. Chen, G. E. W. Bauer, E. Saitoh, and S. T. B. Goennenwein, "Quantitative study of the spin Hall magnetoresistance in ferromagnetic insulator/normal metal hybrids," Phys. Rev. B **87**, 224401 (2013).

127. Y.-T. Chen, S. Takahashi, H. Nakayama, M. Althammer, S. Goennenwein, E. Saitoh, and G. Bauer, "Theory of spin Hall magnetoresistance," Phys. Rev. B **87**, 144411 (2013).

128. S. Meyer, R. Schlitz, S. Geprägs, M. Opel, H. Huebl, R. Gross, and S. T. B. Goennenwein, "Anomalous Hall effect in YIG|Pt bilayers," Appl. Phys. Lett. **106**, 132402 (2015).

129. Y. Lv, J. Kally, T. Liu, P. Sahu, M. Wu, N. Samarth, and J.-P. Wang, "Large unidirectional spin Hall and Rashba-Edelstein magnetoresistance in topological insulator/magnetic insulator heterostructures," arXiv:1806.09066 (2018).

130. G. X. Miao, J. Chang, B. A. Assaf, D. Heiman, and J. S. Moodera, "Spin regulation in composite spin-filter barrier devices," Nat. Commun. **5**, 1–6 (2014).

131. M. A. Tanaka, Y. Shiji, T. Katsuragi, Y. Miyazaki, K. Mibu, K. Kondou, S. Kasai, and T. Ono, "Magnetic and transport properties of spin-filtering tunnel junctions with magnetic insulator La_2NiMnO_6," in *Journal of Physics: Conference Series* (Institute of Physics Publishing, 2010), Vol. 200, p. 62032.